Enterobactin Protonation and Iron Release: Hexadentate Tris-Salicylate Ligands as Models for Triprotonated Ferric Enterobactin[1]

Seth M. Cohen, Michel Meyer, and Kenneth N. Raymond*

Contribution from the Department of Chemistry, University of California, Berkeley, California 94720

Received October 2, 1997

Abstract: Enterobactin mediates iron uptake in *Escherichia coli* and related bacteria. The structure of the neutral protonated ferric enterobactin complex Fe[H_3enterobactin] has been the source of some controversy in the literature. The coordination chemistry of the new model ligands tris[(2-hydroxybenzoyl)-2-aminoethyl]-amine (TRENSAM) and tris[(2-hydroxy-3-methoxybenzoyl)-2-aminoethyl]amine (TREN(3M)SAM) demonstrate the previously proposed tris-salicylate mode of binding for ferric enterobactin; they form 1:1 metal−ligand complexes with Fe^{3+} and Al^{3+} that bind the metals through tris-salicylato coordination (i.e., the chelate is a six-membered metallocycle with the phenolic and amide oxygens binding the metal center). The ferric and aluminum complexes of TRENSAM are isostructural and crystallize in the monoclinic space group $P2_1/c$. The ferric and aluminum complexes of TREN(3M)SAM are nearly isostructural and crystallize in the triclinic space group $P\bar{1}$, with the same salicylate mode of bonding as the TRENSAM complexes. The TRENSAM ligand and its metal complexes have been investigated by NMR, potentiometric, and spectrophotometric techniques, and the results of these experiments are compared to Fe[H_3enterobactin] and a biomimetic analogue Fe[H_3MECAM] (which supports growth of *E. coli*). The properties of Fe[TRENSAM] and Fe[TREN(3M)-SAM] represent an iron release pathway for synthetic analogues of enterobactin that are not susceptible to the degradative pathway usual for enterobactin.

Introduction

Enterobactin (Figure 1), the potent siderophore of enteric bacteria,[2,3] has been the target of study for its chemistry,[4−8] biochemical production,[9−13] and transport and recognition.[14−18] While much is known about the production, structure, and function of enterobactin and its mediation of iron transport into the microbial cell, key steps have remained uncharacterized. Siderophores enter bacterial cells through TonB-dependent outer membrane proteins. The recognition of ferric enterobactin by the FepA receptor protein of *E. coli* was earlier explored by us using synthetic analogues that varied the structure of the ferric

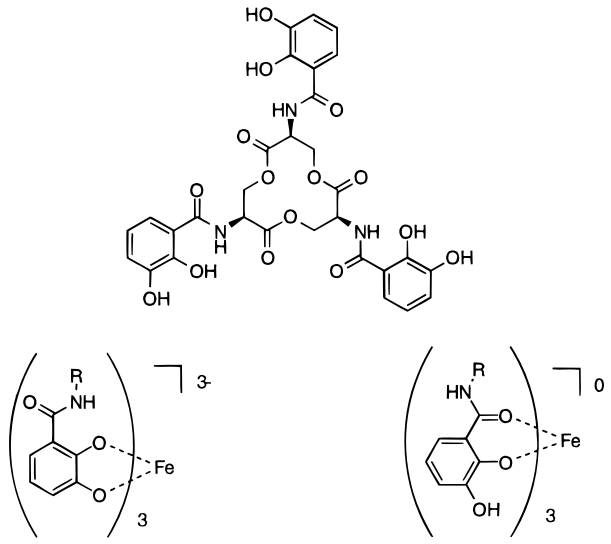

Figure 1. Enterobactin (top) and the two proposed modes for Fe^{3+} chelation: catecholate (bottom left) and salicylate (bottom right).

* To whom correspondence should be addressed.

(1) Paper number 63 in the series "Coordination Chemistry of Microbial Iron Transport." For the previous paper see Telford, J. R. and Raymond, K. N. *J. Biol. Inorg. Chem.*, **1997**, *2*, 750.

(2) Telford, J. R.; Raymond, K. N. in *Comprehensive Supramolecular Chemistry*; Elsevier Science Ltd.: Oxford, 1996; Vol. 1, p 245.

(3) Winkelmann, G. *CRC Handbook of Microbial Iron Chelates*; CRC Press: Boca Raton, 1991.

(4) Isied, S. S.; Kuo, G.; Raymond, K. N. *J. Am. Chem. Soc.* **1976**, *98*, 1763.

(5) Harris, W. R.; Carrano, C. J.; Cooper, S. R.; Sofen, S. R.; Avdeef, A. E.; McArdle, J. V.; Raymond, K. N. *J. Am. Chem. Soc.* **1979**, *101*, 6097.

(6) Scarrow, R. C.; Ecker, D. J.; Ng, C.; Liu, S.; Raymond, K. N. *Inorg. Chem.* **1991**, *30*, 900.

(7) Karpishin, T. B.; Dewey, T. M.; Raymond, K. R. *J. Am. Chem. Soc.* **1993**, *115*, 1842.

(8) Meyer, M.; Telford, J. R.; Cohen, S. M.; White, D.; Xu, J.; Raymond, K. N. *J. Am. Chem. Soc.* **1997**, *119*, 10093.

(9) Walsh, C. T.; Liu, J.; Rusnak, F.; Sakaitani, M. *Chem. Rev.* **1990**, *90*, 1105.

(10) Chenault, S. S.; Earhart, C. F. *Mol. Microbiol.* **1991**, *5*, 1405.

(11) Foster, M. S.; Carroll, J. N.; Niederhoffer, E. C. *FEMS Microbiol. Lett.* **1994**, *117*, 79.

(12) Kwon, O.; Hudspeth, M. E. S.; Meganathan, R. *J. Bacteriol.* **1996**, *178*, 3252.

(13) Hantash, F. M.; Ammerlaan, M.; Earhart, C. F. *Microbiology* **1997**, *143*, 147.

(14) Ecker, D. J.; Matzanke, B. F.; Raymond, K. N. *J. Bacteriol.* **1986**, *167*, 666.

(15) Matzanke, B.; Ecker, D. J.; Yang, T. S.; Huynh, B. H.; Muller, G.; Raymond, K. N. *J. Bacteriol.* **1986**, *167*, 674.

(16) Ecker, D. J.; Loomis, L. D.; Cass, M. E.; Raymond, K. N. *J. Am. Chem. Soc.* **1988**, *110*, 2457.

(17) Armstrong, S. K.; McIntosh, M. A. *J. Biol. Chem.* **1995**, *270*, 2483.

(18) Newton, S. M. C.; Allen, J. S.; Cao, Z.; Qi, Z.; Jiang, X.; Spencel, C.; Igo, J. D.; Foster, S. B.; Payne, M. A.; Klebba, P. E. *Proc. Natl. Acad. Sci. U.S.A.* **1997**, *94*, 4560.

S0002-7863(97)03442-2 CCC: $15.00
Published on Web 06/11/1998

complex,[16] and the key components for molecular recognition were identified. Recent double mutagenesis studies of the FepA receptor[18] have identified a binding site, containing multiple positive charges, that seems consistent with the proposed model.

The terminus of enterobactin's role as a transport agent involves iron release. Relatively recent studies[19] have confirmed an earlier report of an esterase,[20] which is about four times as effective in hydrolyzing the triester serine of the enterobactin free ligand as in hydrolyzing the ferric complex. However, synthetic analogues, which are not susceptible to this hydrolysis, are typically about 5% as effective as enterobactin in delivering iron to the cell.[15] This is still sufficient for significant growth promotion and requires an alternative, if secondary, mechanism for iron release. The measured reduction potential of ferric enterobactin at neutral pH does not allow for release of iron as Fe^{2+}.[5,21] However, protonation of ferric enterobactin makes reduction significantly easier,[22] which has made understanding the solution chemistry and structure of the protonated ferric enterobactin species significant for understanding microbial iron transport.[23] Although some of the literature has been confusing and contradictory, it is now clear that ferric enterobactin undergoes a series of sequential protonation reactions that eventually results in a neutral triprotonated Fe^{3+} enterobactin complex. While solution NMR[23] and FTIR[24] studies supported a "salicylate" coordination model (in which protonation of the meta phenolates led to their replacement in the Fe^{3+} coordination sphere by the amide carbonyl oxygens) there were no direct structural analogues to confirm this model. Prompted by the importance of understanding how bacterial pathogens obtain iron from all sources[25,26] and the previous confusion in the literature, we have developed direct analogues of the protonated enterobactin complex, determined their structure by X-ray diffraction, and related their spectroscopic properties and those of the siderophore and other growth-supporting analogues.

Results

Syntheses. The syntheses of TRENSAM and TREN(3M)SAM are shown in Schemes 1 and 2, respectively.

Metal complexes of either TRENSAM or TREN(3M)SAM were formed by using identical methodologies. The ligand was dissolved in methanol, and the anhydrous metal chloride salt was added along with pyridine as base. Complexes prepared in this fashion form as the hydrochloride salt with the protonated bridgehead TREN nitrogen bearing the positive charge. Positive ion fast atom bombardment mass spectrometry (FAB) showed the molecular peaks of the mononuclear 1:1 ligand-to-metal complexes for the TRENSAM complexes. No peaks corresponding to a complex having a 2:1 ligand-to-metal stoichiometry were observed. Unambiguous determination of the salicylate mode of binding was obtained from the X-ray structure determination of both the ferric and aluminum complexes of TRENSAM and TREN(3M)SAM.

Scheme 1

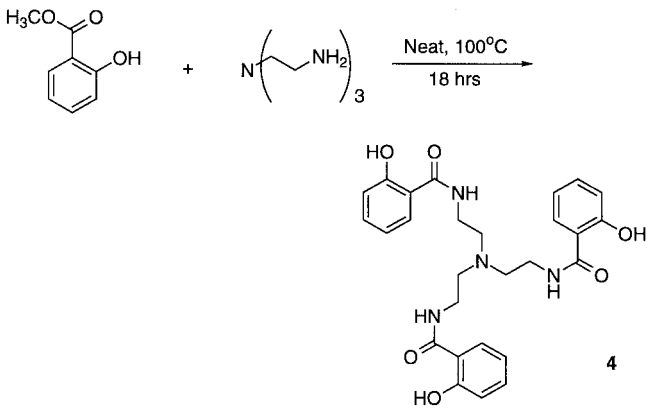

X-ray Structures of M^{3+}[TRENSAM] ($M^{3+} = Fe^{3+}$, Al^{3+}). The structure of Fe[TRENSAM] is shown in Figure 2. The ferric complex crystallized in the centrosymmetric space group $P2_1/c$ as a 1:1 metal-to-ligand complex hydrochloride salt, with one molecule of methanol in the asymmetric unit (Table 1). The tertiary nitrogen of the TREN scaffold is protonated, giving the complex a positive charge, with chloride as the counteranion. The complex deviates from ideal C_{3v} symmetry in two significant ways: (1) two of the bidentate ligands are positioned closer to each other than to the third, as viewed down the pseudo-3-fold axis; and (2) the chelate rings twist in order to maintain a pseudooctahedral coordination environment around the ferric center (Figure 3). Consequently, the dihedral angles between the carbonyl oxygens and the phenoyl rings differ for each chelate ring (Table 3). While one of the chelate rings is nearly planar (dihedral angle 2.9°), the other two deviate significantly from planarity, with dihedral angles at 18.0° and 28.9°, respectively. The negatively charged phenolate oxygens are more tightly held to the metal center than the amide oxygens, with an average M−O bond length of 1.92 Å, while the amide oxygens have an average M−O bond length of 2.07 Å.

The corresponding aluminum complex (Figure 2) is nearly isostructural with the ferric complex (Table 1). The dihedral chelate angles are similar to that of the Fe[TRENSAM] (Table 3). The average bond lengths in the aluminum complex are 1.83 Å for the phenolic oxygen and 1.94 Å for the carbonyl oxygen. These differ by 0.09 and 0.13 Å respectively from Fe[TRENSAM], in good agreement with the difference in atomic radii of Al^{3+} and Fe^{3+}.[27]

X-ray Structures of M^{3+}[TREN(3M)SAM] ($M^{3+} = Fe^{3+}$, Al^{3+}). X-ray quality crystals of the ferric complex were obtained as purple blocks from methanol by diffusion with diethyl ether (Table 2). The ligand binds the iron cation via three salicylate chelate rings (Figure 4). The TREN nitrogen is protonated, and Fe[TREN(3M)SAM] crystallizes as the hydrochloride salt. The metal−oxygen bond lengths in Fe[TREN(3M)SAM] are comparable to those in Fe[TRENSAM], but the dihedral twist angles of the chelate oxygens differ significantly. These also vary substantially between the two different complexes in the asymmetric unit of the crystal structure (Table 3).

Suitable single crystals of Al[TREN(3M)SAM] were obtained from saturated methanolic solutions of the complex diffused with pentane. The complex crystallized as the hydrochloride salt, with an additional pyridinium chloride salt pair (Table 2). Like the other complexes Al[TREN(3M)SAM] is a tris-salicylate complex, as shown in Figure 4. The metal−oxygen bond length differences observed between Fe[TRENSAM] and Al[TREN-

(19) Brickman, T. J.; McIntosh, M. A. *J. Biol. Chem.* **1992**, *267*, 12350.
(20) O'Brien, I. G.; Cox, G. B.; Gibson, F. *Biochim. Biophys. Acta* **1971**, *237*, 537.
(21) Cooper, S. R.; McArdle, J. V.; Raymond, K. N. *Proc. Natl. Acad. Sci. U.S.A.* **1978**, *75*, 3551.
(22) Lee, C.-W.; Ecker, D. J.; Raymond, K. N. *J. Am. Chem. Soc.* **1985**, *107*, 6920.
(23) Cass, M. E.; Garrett, T. M.; Raymond, K. N. *J. Am. Chem. Soc.* **1989**, *111*, 1677.
(24) Pecoraro, V. L.; Harris, W. R.; Wong, G. B.; Carrano, C. J.; Raymond, K. N. *J. Am. Chem. Soc.* **1983**, *105*, 4623.
(25) Gross, R. *FEMS Microbiol. Rev.* **1993**, *104*, 301.
(26) Wooldridge, K. G.; Williams, P. H. *FEMS Microbiol. Rev.* **1993**, *12*, 325.
(27) Shannon, R. D. *Acta Crystallogr.* **1976**, *A32*, 751.

Scheme 2

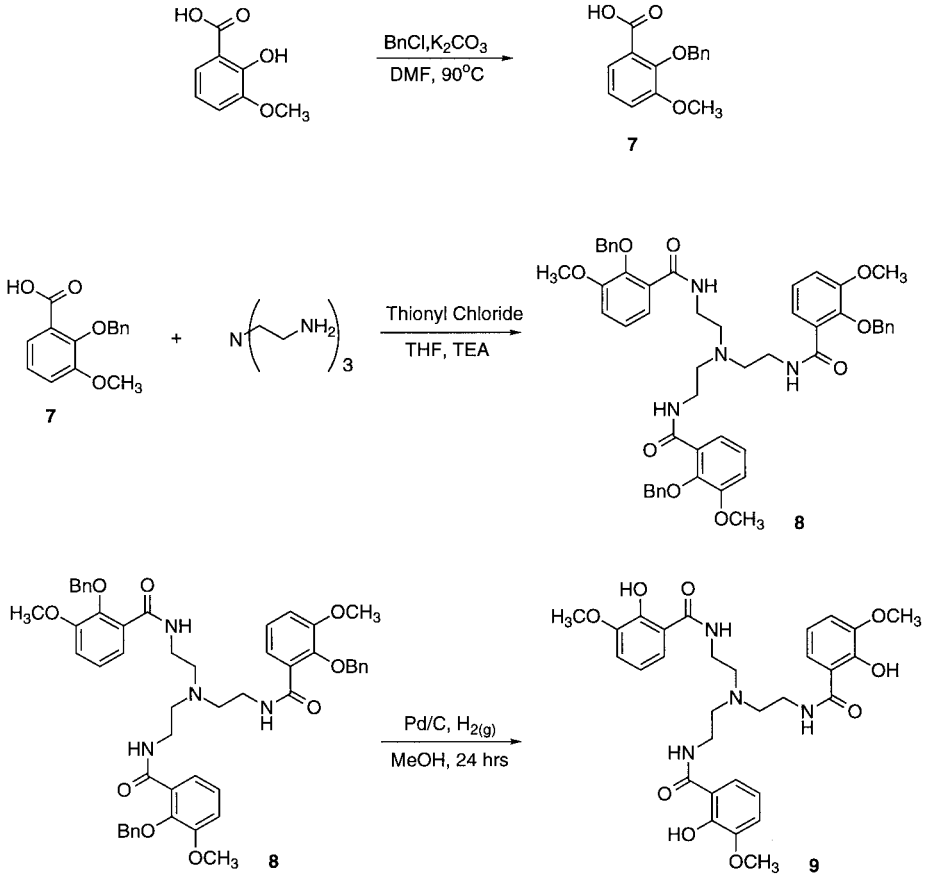

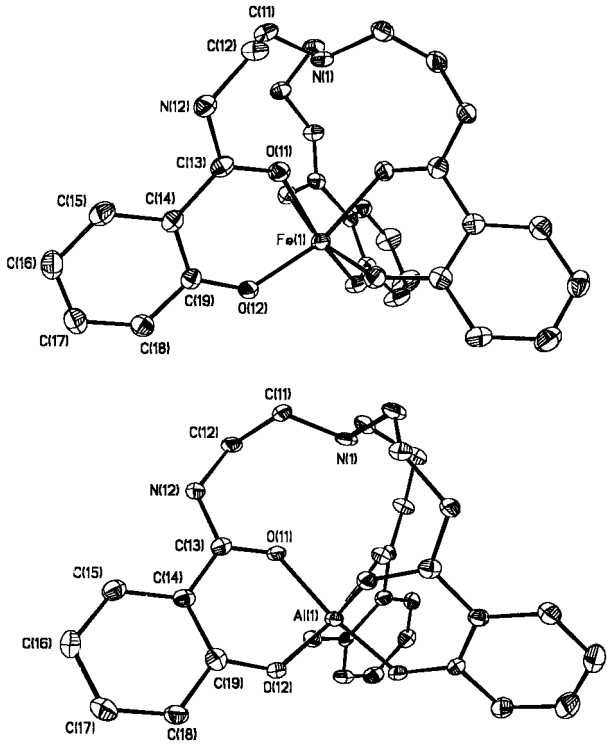

Figure 2. Structural (ORTEP) diagrams of Fe[TRENSAM] (top) and Al[TRENSAM] (bottom) viewed perpendicular to the approximate 3-fold axis (50% probability ellipsoids). Hydrogen atoms, counterion, and solvent have been omitted for clarity.

SAM] are maintained between Fe[TREN(3M)SAM] and Al-[TREN(3M)SAM].

Table 1. Crystal Data and Structure Refinement for Fe[TRENSAM] and Al[TRENSAM]

	Fe[TRENSAM]	Al[TRENSAM]
empirical formula	$FeC_{28}H_{32}N_4O_7Cl$	$AlC_{28}H_{32}N_4O_7Cl$
formula weight	627.88	599.01
temperature, K	179(2)	176(2)
crystal system	monoclinic	monoclinic
space group	$P2_1/c$	$P2_1/c$
a, Å	12.7556(2)	12.5617(3)
b, Å	13.0250(2)	13.0506(2)
c, Å	17.59310(10)	17.5437(5)
β, deg	107.8700(10)	107.9780(10)
vol, Å^3, Z	2781.93(6), 4	2735.65(11), 4
density(calcd), g cm^{-3}	1.499	1.454
crystal size, mm	0.09 × 0.15 × 0.20	0.03 × 0.10 × 0.30
no. of reflcns collected	11397	11110
no. of independent reflcns	3994 [R(int) = 0.0362]	3901 [R(int) = 0.0633]
data/restraints/parameters	3989/0/376	3901/0/374
GOF	1.105	1.091
final R indices [$I > 2\sigma(I)$]	$R_1 = 0.0361$, $wR_2 = 0.0775$	$R_1 = 0.0563$, $wR_2 = 0.1070$
R indices (all data)	$R_1 = 0.0486$, $wR_2 = 0.0856$	$R_1 = 0.0932$, $wR_2 = 0.1231$
largest diff peak and hole, e Å^{-3}	0.250 and −0.310	0.266 and −0.294

FTIR Spectroscopy. The infrared spectra of TRENSAM and TREN(3M)SAM exhibit a shift of the carbonyl amide stretching frequencies to lower wavenumbers upon complexation of Al^{3+} or Fe^{3+}. For TRENSAM the carbonyl stretch for the free ligand (1636 cm^{-1}) shifts to lower energy by 21 and 31 cm^{-1} for the Al^{3+} and the Fe^{3+} complexes, repectively. Likewise, for TREN(3M)SAM the carbonyl stretch (1635 cm^{-1}) shifts 25 and 43 cm^{-1} in the Al^{3+} and Fe^{3+} complexes,

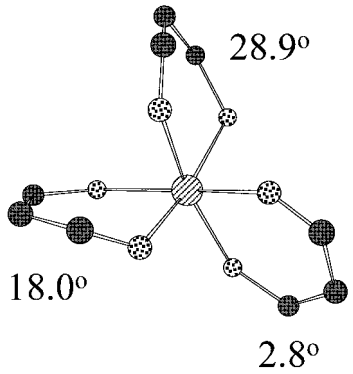

Figure 3. Ball and stick diagram of the coordination sphere of Fe[TRENSAM] showing the twist in the salicylate chelate rings.

Table 2. Crystal Data and Structure Refinement for Fe[TREN(3M)SAM] and Al[TREN(3M)SAM]

	Fe-[TREN(3M)SAM]	Al-[TREN(3M)SAM]
empirical formula	$FeC_{35}H_{49}N_{4.5}O_{12.75}Cl$	$AlC_{37}H_{48}N_5O_{11}Cl$
formula weight	828.09	836.68
temperature, K	171(2)	164(2)
crystal system	triclinic	triclinic
space group	$P\bar{1}$	$P\bar{1}$
a, Å	14.2837(3)	10.0967(2)
b, Å	16.2155(3)	14.5189(3)
c, Å	18.69920(10)	15.6818(2)
α, deg	77.5480(10)	63.1540(10)
β, deg	67.7880(10)	76.6750(10)
γ, deg	75.2560(10)	70.9100(10)
vol, Å^3, *Z*	3842.99(11), 4	1968.78(6), 2
density (calcd), g cm^{-3}	1.431	1.411
crystal size, mm	0.10 × 0.20 × 0.20	0.10 × 0.20 × 0.20
no. of reflcns collected	16144	9524
no. of independent reflcns	10781 [*R*(int) = 0.0548]	6608 [*R*(int) = 0.0247]
data/restraints/parameters	10772/0/1009	6606/0/509
GOF	1.176	1.117
final *R* indices [$I > 2\sigma(I)$]	$R_1 = 0.0793$, $wR_2 = 0.1829$	$R_1 = 0.0446$, $wR_2 = 0.1028$
R indices (all data)	$R_1 = 0.1180$, $wR_2 = 0.2295$	$R_1 = 0.0542$, $wR_2 = 0.1133$
largest diff peak and hole, e Å^{-3}	0.911 and −0.510	0.773 and −0.660

respectively. These observations support the earlier assignments for this mode of coordination.[24]

^{13}C NMR Study of the Aluminum(III) Complexes. Comparison of TRENSAM with Al[TRENSAM] shows significant differences in their ^{13}C NMR spectra obtained in CD_3OD. Carbon atoms attached to heteroatoms involved in metal binding are deshielded relative to the free ligand. The carbonyl and phenolic carbon signals each experience a downfield shift (3.2 and 6.5 ppm respectively), suggesting that in solution the amide and phenol oxygen atoms participate in metal binding.

The ^{13}C NMR spectrum of Al[TREN(3M)SAM] shows the same trend as that seen for Al[TRENSAM]. Comparison of Al[TREN(3M)SAM] with that of TREN(3M)SAM (both taken in DMSO-d_6) also shows downfield shifts for the carbonyl and phenolic carbons (1.5 and 6.1 ppm) attributed to metal binding in solution.

^{1}H NMR Study of Al[TRENSAM]. The ^{1}H NMR spectrum of Al[TRENSAM] in CD_3OD shows a single set of resonances, suggesting a C_{3v} symmetric complex on the NMR time scale. The four sharp resonances in the aromatic region are only slightly shifted compared to the free ligand. In contrast, the two pairs of methylene protons, which appear as two triplets in the spectrum of the free ligand, are shifted downfield and become magnetically inequivalent, forming an AA′XX′ system. At room temperature three broad peaks (integrating as 6:3:3)

Table 3. Selected Bond Lengths (Å), Dihedral Angles (deg), and Atomic Distances (Å) for the M^{3+}[TRENSAM] and M^{3+}[TREN(3M)SAM] Structures (M^{3+} = Fe^{3+} and Al^{3+})

complex	chelate dihedral angles[a]	carbonyl−metal bond length[b]	phenolic−metal bond length[b]	carbonyl−amine distance[c,d]
Fe[TRENSAM]	2.9	2.06	1.91	2.92
	18.0	2.03	1.92	3.48 (3.09)
	28.9	2.12	1.94	2.86
Al[TRENSAM]	0.3	1.93	1.82	2.94
	14.0	1.91	1.83	3.40 (3.07)
	26.8	1.99	1.84	2.87
Fe[TREN(3M)SAM][e]	16.2	2.06	1.91	3.09
	19.3	2.09	1.92	3.07 (3.06)
	22.7	2.10	1.93	3.03
	8.5	2.04	1.92	3.14
	20.0	2.08	1.91	2.88 (3.03)
	27.9	2.10	1.92	3.06
Al[TREN(3M)SAM]	10.7	1.92	1.81	2.88
	11.4	1.90	1.84	3.12 (3.00)
	14.3	1.93	1.82	3.00

[a] See Figure 3. [b] Numbers represent metal-to-oxygen distances. [c] Numbers in parantheses denote averages. [d] Numbers represent oxygen-to-nitrogen (TREN bridgehead nitrogen) distances. [e] Fe[TREN(3M)SAM] crystallizes with two conformationally distinct molecules in the asymmetric unit.

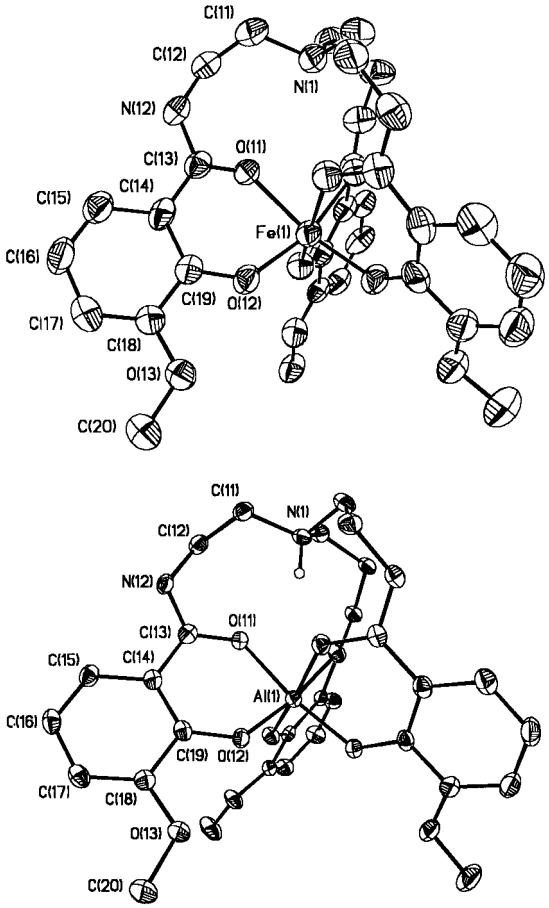

Figure 4. Structural (ORTEP) diagrams of Fe[TREN(3M)SAM] (top) and Al[TREN(3M)SAM] (bottom) perpendicular to the approximate 3-fold axis (50% probability ellipsoids). The ORTEP diagram for Al[TREN(3M)SAM] shows the proton on the TREN bridgehead nitrogen. Hydrogen atoms, counterion, and solvent have been omitted for clarity.

are observed at 3.47, 3.79, and 4.15 ppm. The Al[TRENSAM] complex is chiral and forms a racemic mixture of both Λ and Δ enantiomers. Based on the large splitting ($\Delta\nu = 103.5$ Hz) induced by the proximity of the chiral metal center, the resonances at 3.79 and 4.15 ppm are assigned to the methylene protons adjacent to the amide group. The broadness of the methylene atom resonances reveals a site exchange of the two diastereotopic protons due to the interconversion of both enantiomers. This dynamic process was analyzed by variable-temperature ^{1}H NMR spectroscopy in CD_3OD. At 265 K, the two broad lines centered at 3.79 (δ_A) and 4.15 ppm ($\delta_{A'}$) resolve as doublets of doublets, while the multiplet at 3.47 ppm shows second-order effects. The coupling constants derived from the AA′ part ($^2J_{AA'} = 15.2$ Hz, $^3J_{AX'} = 8.9$ Hz, $^3J_{A'X} = 8.8$ Hz, $^3J_{AX}$ and $^3J_{A'X'} < 2$ Hz) suggest a conformation for which the dihedral angles between protons A and X and protons A′ and X′ are close to 90°. This agrees well with the calculated hydrogen positions as determined by single-crystal X-ray diffraction. In the structure of Al[TRENSAM] the dihedral angles between the A and X, and A′ and X′ hydrogen atoms range from 87.3° to 90.2°. Upon heating a discrete exchange pattern is observed. Resonances A and A′ display line broadening, coalesce at $T_c = 320$ K, and merge into a single resonance at higher temperatures. Assuming the site exchange is slow compared to the NMR time scale at the coalescence temperature, the activation barrier for the inversion of configuration of Λ- and Δ-Al[TRENSAM] is 61.9 kJ mol^{-1} (calculated according to the formula $\Delta G^{\ddagger} = (19.13 \times 10^{-3})T_c(9.62 + \log T_c - \log \Delta\nu)$ with $\Delta\nu = 103.5$ Hz).

UV−Vis Spectroscopy. The absorption spectra in neutral aqueous media of ferric TRENSAM and TREN(3M)SAM complexes exhibit two well-resolved $\pi \rightarrow \pi^*$ transitions in the UV region at 279 ($\epsilon = 13\,600$ M^{-1} cm^{-1}) and 301 nm ($\epsilon = 13\,300$ M^{-1} cm^{-1}) for Fe[TRENSAM] and at 288 ($\epsilon = 9\,800$ M^{-1} cm^{-1}) and 314 nm ($\epsilon = 10\,100$ M^{-1} cm^{-1}) for Fe[TREN(3M)SAM]. The low-energy bands show a shoulder at higher wavelengths. The broad absorption maximum in the visible is due to ligand-to-metal charge-transfer transitions responsible for the orange color of Fe[TRENSAM] ($\lambda = 455$ nm, $\epsilon = 5600$ M^{-1} cm^{-1}) and the purple color of Fe[TREN(3M)SAM] ($\lambda = 492$ nm, $\epsilon = 4700$ M^{-1} cm^{-1}). The spectroscopic data for Fe[TRENSAM] are in agreement with those reported for the related complex from an FTIR study (Fe[MESAM], $\lambda = 468$ nm).[24] Diffuse reflectance spectra of crystalline material suggest a similar coordination environment in both solid state and solution: the absorption maximum in a barium sulfate matrix shifts to ∼470 and 547 nm for Fe[TRENSAM] and Fe[TREN(3M)SAM], respectively.

Ligand Protonation Constants. The protonation constants defined by eq 1 (the charge on the ligand is omitted) for the monochelate model compound MSAM (2-hydroxybenzoylaminomethane), and the tripods TRENAC (tris(acetamide-2-aminoethyl)amine), Me-TRENSAM (tris[(2-methoxybenzoyl)-2-aminoethyl]amine), and TRENSAM were determined by potentiometric and spectrophotometric titrations. The average values together with the corresponding standard deviations are reported in Table 4.

$$LH_{n-1} + H^+ \rightleftarrows LH_n$$

$$K_{01n} = \frac{[LH_n]}{[LH_{n-1}][H^+]} \qquad (1)$$

The protonation constant of MSAM determined by potentiometry (log $K_{011} = 8.03(1)$) and absorption spectroscopy (log $K_{011} = 7.93(1)$) are in good agreement. Compared with phenol (log $K_{011} = 9.89$) and salicylic acid (log $K_{011} = 13.4$), MSAM is more acidic. The broad UV absorption band of the deprotonated species ($\lambda = 325$ nm, $\epsilon = 5700$ M^{-1} cm^{-1}) shifts upon protonation ($\lambda = 297$ nm, $\epsilon = 3500$ M^{-1} cm^{-1}). Three sharp isosbestic points are observed at 243, 258, and 304 nm.

Two nonchelating tripods, TRENAC and the methyl-protected derivative of TRENSAM, Me-TRENSAM, were prepared in order to model the protonation properties of TRENSAM's tertiary amine. For TRENAC, the log K_{011} values measured by potentiometry and spectrophotometry are 5.98(1) and 6.03(1), respectively. Spectrophotometric titrations showed that there is no spectral contribution above 240 nm from the aliphatic amine or amide $n \rightarrow \pi^*$ and/or $\pi \rightarrow \pi^*$ transitions upon protonation/deprotonation. Due to limited solubility in water, Me-TRENSAM was titrated at low concentration (2.3 μM) by monitoring the spectral changes as a function of p[H]. The study of this tripod indicated that protonation of the single basic site, the bridgehead amine, influences significantly the $\pi \rightarrow \pi^*$ absorption bands of the 2-methoxysalicylamide groups. The absorption band centered at 290 nm ($\epsilon = 7100$ M^{-1} cm^{-1}) at high p[H] is slightly shifted toward the red ($\lambda = 294$ nm) as p[H] decreases, with a concomitant hyperchromic effect ($\epsilon = 8200$ M^{-1} cm^{-1}). Simultaneously, the high-energy shoulder emerges at lower p[H] ($\lambda = 232$ nm, $\epsilon = 24\,500$ M^{-1} cm^{-1}). These variations allowed accurate estimation of the amine protonation constant: log $K_{011} = 6.01(7)$. The four or five log unit shift of pK_a for the tertiary amine of TRENAC and Me-TRENSAM is characteristic of the hydrogen bonding in such ligands; in the deprotonated state the amide hydrogen atoms form a five-membered hydrogen-bonded chelate ring with the lone pair of the central nitrogen.

TRENSAM has four protonation sites, three phenolic groups, and the tertiary amine. The solubility limit is approximately 60 μM in the p[H] range 5−7. Thus, 50 μM solutions of TRENSAM were titrated with 0.01 M HCl containing 0.09 M KCl. The average log K values refined for four independent experiments are listed in Table 4. Since the concentration conditions correspond to the lower limit of reliability of the potentiometric method, the ligand's protonation was also studied spectrophotometrically by taking advantage of the intense UV absorption bands of the salicylate functionality. Representative absorption spectra obtained for TRENSAM are shown in Figure 5. At high p[H], the extinction coefficient of the intense UV absorption band ($\lambda = 327$ nm, $\epsilon = 17\,000$ M^{-1} cm^{-1}) for TRENSAM is three times the value for the corresponding monomer, MSAM. Similarly, the band decreases in intensity and shifts to shorter wavelengths ($\lambda = 300$ nm) as the p[H] is lowered down to 7.9. These spectral changes correspond to overlapping protonation equilibria. As the p[H] is further decreased, the low-energy tail of the absorption band disappears

Table 4. Protonation Constants of MSAM, Me-TRENSAM, and TRENSAM[a]

	MSAM	Me-TRENSAM	TRENSAM	
log K_{011}	8.03(1)	6.01(7)	9.19(5)[c]	9.1(2)[d]
log K_{012}			8.86(6)[c]	8.9(1)[d]
log K_{013}			7.17(8)[c]	7.4(1)[d]
log K_{014}			5.80(10)[c]	6.0(1)[d]
log K_{av}[b]			7.39	7.5

[a] $I = 0.1$ (KCl), $T = 25$ °C. Numbers in parentheses correspond to the estimated standard deviations calculated from the variance/covariance matrix of at least three independent measurements. [b] The average does not include the protonation of the amine (log K_{012}). [c] Potentiometric measurements. [d] Spectrophotometric measurements.

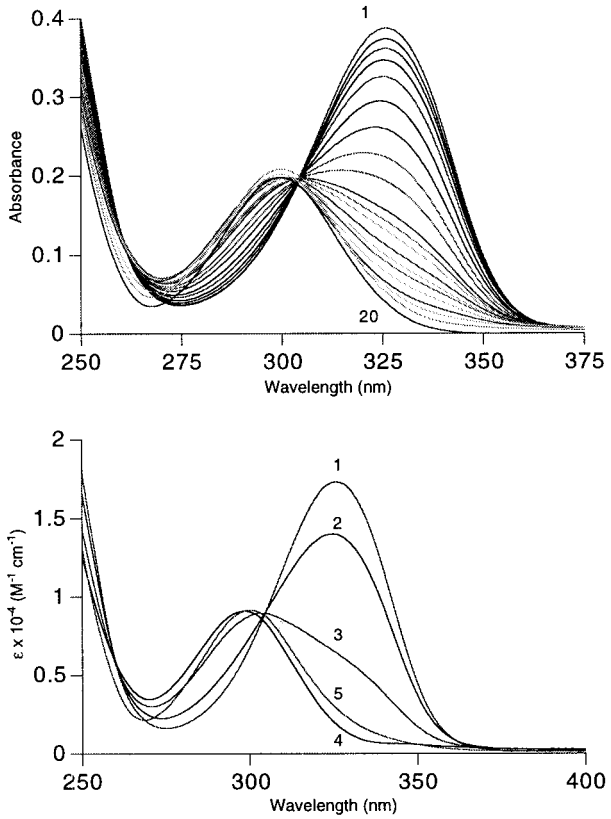

Figure 5. Spectrophotometric titration (top) of TRENSAM by HCl in water. $I = 0.1$ (KCl), $T = 25.0(2)$ °C, $l = 10$ cm, [TRENSAM] = 2.24 μM, [HCl] = 0.100 M, p[H] = 10.97, 10.18, 9.81, 9.58, 9.37, 9.16, 8.96, 8.76, 8.56, 8.19, 8.01, 7.85, 7.54, 7.36, 7.22, 7.04, 6.72, 5.61, 3.72, 2.45 (spectra 1 to 20). Calculated absorption spectra (bottom) of the protonated species of TRENSAM in water: 1, L^{3-}; 2, LH^{2-}; 3, LH_2^-; 4, LH_3; 5, LH_4^+. $I = 0.1$ (KCl), $T = 25.0(2)$ °C.

while the maximum remains almost unchanged. Factor analysis of the entire data set comprising about 60 spectra between p[H] 11 and 2.5, and 151 wavelengths for each replicate, indicated a minimum of three and possibly four absorbing species. The best refinement with the nonlinear least-squares program REFSPEC[28] was obtained with the model including five species: L^{3-}, LH^{2-}, LH_2^-, LH_3, and LH_4^+. The calculated absorption spectra are depicted in Figure 5. The LH_3 and LH_4^+ species exhibit almost identical spectroscopic properties. The refined constants, included in Table 4, are in good agreement with the values determined by potentiometry. As previously observed for a variety of tripodal sequestering agents,[29−34] the average protonation constants of the phenol groups are distributed around the pK_a value of the bidentate model ligand, MSAM. The stepwise protonation constants are about equally spaced around the average value of 8.0, the differences $\log K_{011} - \log K_{013} = 1.9$ and $\log K_{013} - \log K_{014} = 1.1$ being much larger than the statistical factor of log 3.

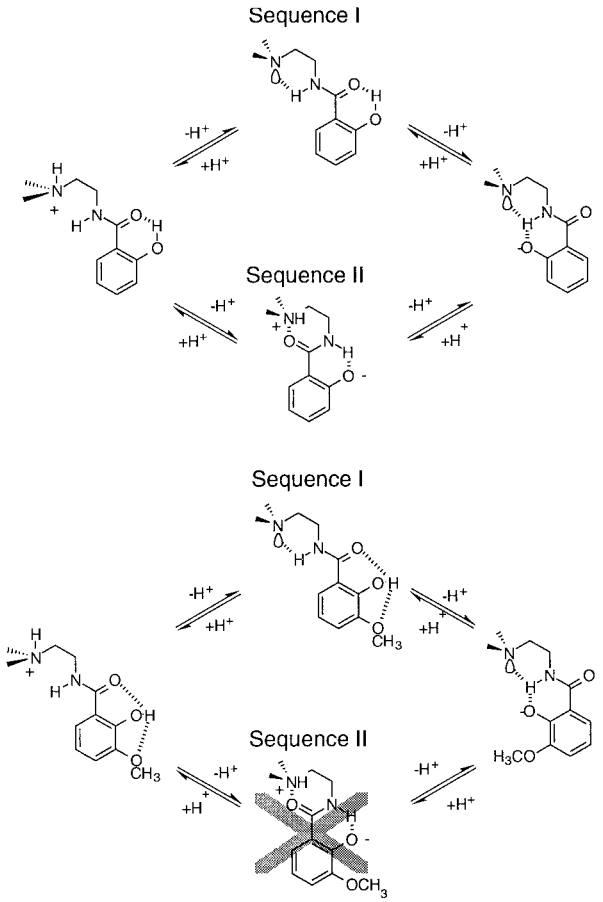

Figure 6. Deprotonation schemes of TRENSAM (top) and TREN(3M)SAM (bottom) showing the hydrogen bond networks. For TRENSAM, two sequences are consistent with the protonation data. However, for TREN(3M)SAM the ^{1}H NMR data show that sequence I, with three hydrogen bonds, is favored.

The second protonation constant is assigned to the protonation of the bridgehead amine, although direct evidence could not be gained from an NMR titration due to the limited solubility of TRENSAM in D_2O. Compared with TRENAC and Me-TRENSAM, the tertiary amine is three log units more basic. This can be understood in terms of the most stable hydrogen bond network as illustrated in Figure 6. In TRENSAM, following sequence I (tertiary amine deprotonates first) or sequence II (one phenol unit deprotonates first) leads to hydrogen bond networks of comparable stabilities. Since the relative acidity of the capping amine is related to its ability to interact with the amide hydrogen atoms through hydrogen bonds in the deprotonated state, a higher pK_a value is expected for TRENSAM. It follows that the corresponding protonation constant of TREN(3M)SAM should be comparable to the values found for TRENAC and Me-TRENSAM. Indeed, the hydrogen bond network available following sequence I (Figure 6) is by far more stable, since the alternative pathway II leads only to two (vs three) centered H-bonds. This prediction is fully supported by the ^{1}H NMR results shown in Figure 7. Between p[D] 6 and 8, the methylene protons H_a and H_b undergo the largest shift with an inflection point at p[D] 6.9(1). This behavior is consistent with the deprotonation of the central amine, and is in close agreement with the predicted value of 6.3(1) when corrected for the deuterium effect.[35] The second buffer region observed between p[D] 9.5 and 11 is associated

(28) Turowski, P. N.; Rodgers, S. J.; Scarrow, R. C.; Raymond, K. N. *Inorg. Chem.* **1988**, *27*, 474.
(29) Serratrice, G.; Mourral, C.; Zeghli, A.; Beguin, C. G.; Baret, P.; Pierre, J. L. *New J. Chem.* **1994**, *18*, 749.
(30) Serratrice, G.; Zeghli, C. G.; Gellon, G.; Baret, P.; Pierre, J. L. *J. Chim. Phys.* **1992**, *89*, 549.
(31) Ng, C. Y.; Rodgers, S. J.; Lee, C. W.; Raymond, K. N. *Inorg. Chem.* **1989**, *28*, 2062.
(32) Rodgers, S. J.; Lee, C. W.; Ng, C. Y.; Raymond, K. N. *Inorg. Chem.* **1987**, *26*, 1622.
(33) Caris, C.; Baret, P.; Pierre, J. L.; Serratrice, G. *Tetrahedron* **1996**, *52*, 4659.
(34) Xu, J.; Frankin, S. J.; Whisenhunt, D. W., Jr.; Raymond, K. N. *J. Am. Chem. Soc.* **1995**, *117*, 7245.
(35) Delgado, R.; Frausto Da Silva, J. J. R.; Amorim, M. T. S.; Cabral, M. F.; Chaves, S. *J. Anal. Chim. Acta* **1991**, *245*, 271.

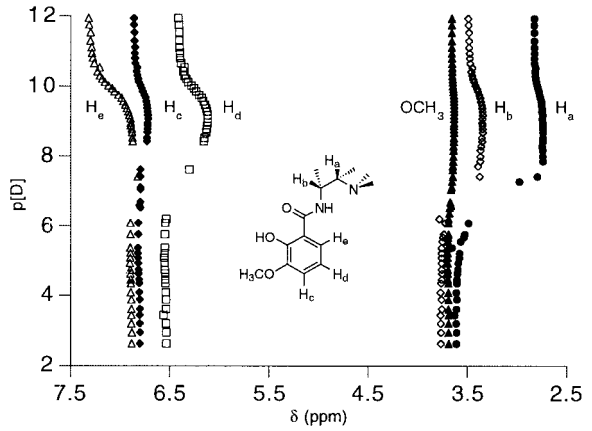

Figure 7. Variations of the ^{1}H NMR chemical shifts recorded at 300 MHz for the nondissociable protons of TREN(3M)SAM in D_2O as a function of p[D]. $T = 23.0(5)$ °C.

with the deprotonation of the phenolic oxygen atoms. The H_e protons sense a change of environment corresponding with a change of conformation of the amide group and a 180° rotation of the aromatic ring as supposed in sequence I (Figure 6). The shift from a *cis* to a *trans* conformation of the amide group is also supported by concomitant downfield shifts of the methylene resonances.

Stability of Ferric TRENSAM. The spectrophotometric titration of Fe[TRENSAM] from p[H] 5.28 to 2.13 and between 250 and 650 nm is shown in Figure 8. Increasing the p[H] above 7 resulted in total disappearance of the charge-transfer band due to formation of iron hydroxide. The complex is stable only in neutral to slightly acidic (p[H] $\sim$ 4.5) conditions. As the p[H] is lowered, the intensity of the LMCT band decreases and finally vanishes around p[H] = 2.3. In contrast to Fe[MESAM], no shift of the absorption band is observed. At p[H] 2.5, both intense $\pi \rightarrow \pi^*$ transitions resolve as a single band ($\lambda = 301$ nm, $\epsilon = 10\,300$ M^{-1} cm^{-1}), the final spectrum being identical to the spectrum calculated for the LH_4^+ species. Isosbestic points are observed in the plot of the first-derivative spectra also shown in Figure 8, suggesting the presence of only two absorbing species, which was confirmed by factor analysis.

The nonlinear least-squares refinement of the overall formation constant β_{11h} defined by eq 2 included the four protonation constants derived from spectrophotometric titrations (Table 4) and the metal hydrolysis products, whose equilibrium constants were fixed to the literature values ($\log \beta_{10-1} = -2.61$, $\log \beta_{10-2} = -5.66$, $\log \beta_{20-2} = 2.86$) and which do not absorb significantly.[36]

$$m\mathrm{Fe}^{3+} + l\mathrm{L}^{n-} + h\mathrm{H}^{+} \overset{\beta_{mlh}}{\rightleftarrows} \mathrm{Fe}_m\mathrm{L}_l\mathrm{H}_h^{\,3m-nl+h}$$

$$\beta_{mlh} = \frac{[\mathrm{Fe}_m\mathrm{L}_l\mathrm{H}_h^{\,3m-nl+h}]}{[\mathrm{Fe}^{3+}]^m[\mathrm{L}^{n-}]^l[\mathrm{H}^+]^h} \qquad (2)$$

The low solubility of the ferric complex in water prevented the unambiguous determination by potentiometry of the stability constant β_{11h} and of the corresponding chemical model. Since the collected spectrophotometric data do not determine a priori if the tertiary amine of ferric TRENSAM remains protonated under the experimental conditions used, two different models were tested. The first assumes that the amine is deprotonated in solution ($\log \beta_{110} = 25.34(7)$), and the second assumes the amine remains protonated ($\log \beta_{111} = 28.39(9)$). For three independent replicates, the first model led systematically to a statistically significant better adjustment (F-test at the 95% confidence level). The deprotonation of Fe[TRENSAM] upon dissolution is also supported by its low solubility. The $\log \beta_{110}$ value is also in excellent agreement with the stability constant of triprotonated ferric MECAM ($\log \beta_{113} = 25.27$), which supports the proposed tris-salicylate structure of its protonated Fe(III) complex.[37]

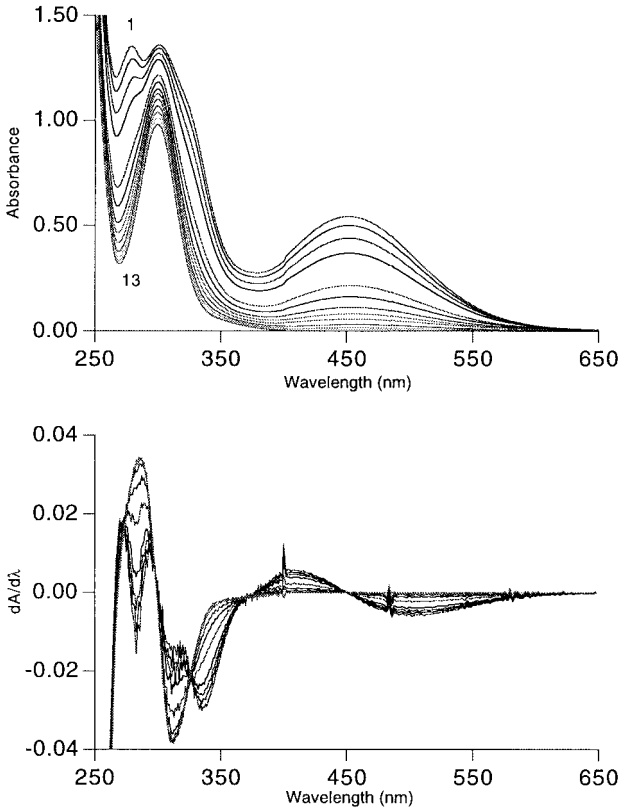

Figure 8. Spectrophotometric titration (top) and first derivative plot (bottom) of Fe[TRENSAM] by HCl in water. The irregular shape of the derivative spectra at 400 and 480 nm is due to small discontinuities in the absorbance plot created by the spectrometer, which are amplified in the derivative plot. $I = 0.1$ (KCl), $T = 25.0(2)$ °C, $l = 10$ cm, [Fe[TRENSAM]] = 10.4 μM, [HCl] = 0.100 M, p[H] = 5.28, 3.92, 3.58, 3.34, 3.11, 3.00, 2.88, 2.77, 2.69, 2.59, 2.48, 2.37, 2.13 (spectra 1 to 13).

Discussion

The TRENSAM ligand system was designed in order to explore the structural and spectroscopic features of a tris-salicylato podand. The structure of Fe[TRENSAM] unambiguously demonstrates the salicylate mode of binding. The structure of Al[TRENSAM] demonstrates the persistance of the salicylato bonding for closely related metal cations.

Despite the structural identification of a salicylate binding mode, the UV and visible spectrum of Fe[TRENSAM] did not correlate well with that of Fe[H_3enterobactin]. To obtain a better model TREN(3M)SAM was synthesized (Scheme 2). Addition of the 3-methoxy substitutent provided an excellent spectroscopic model. The purple color of this complex ($\lambda = 492$ nm) is shifted 37 nm relative to Fe[TRENSAM] ($\lambda = 455$ nm). This correlates well with the purple precipitates associated with Fe[H_3MECAM] and Fe[H_3enterobactin] [5,38] and their UV spectra

(36) Perrin, D. D.; Dempsey, B. *Buffers for pH and Metal Ion Control*; Chapman and Hall: London, 1974.

(37) Harris, W.; Raymond, K. N. *J. Am. Chem. Soc.* **1979**, *101*, 6534.

(38) Loomis, L. D.; Raymond, K. N. *Inorg. Chem.* **1991**, *30*, 906.

($\lambda = 314$ nm) which are nearly identical.[38] Crystal structures of the ferric and aluminum complexes confirm that TREN(3M)SAM also employs a salicylate mode of binding. The methylated phenolic oxygen in TREN(3M)SAM is a donor comparable to the protonated 3-hydroxyl oxygen in Fe[H_3enterobactin]; the structure of Fe[TREN(3M)SAM] is an important confirmation that the protonated phenolic oxygen is not coordinated to Fe^{3+} in Fe[H_3enterobactin].

Formation of a tris-salicylato complex was earlier questioned based on predicted strain in the ligand. Calculations for Fe[H_3MECAM], in both the catecholate and salicylate modes of binding, were interpreted as showing that the crowding of the carbonyl oxygens (and their lone pairs) with the benzene ring would prevent formation of a salicylate complex.[39,40] However, this is contradicted by the structures of M^{3+}[TRENSAM] and M^{3+}[TREN(3M)SAM], which demonstrate the structural integrity of tris-salicylate complexes. The average distance of the carbonyl oxygens to the tertiary amine in the complexes is 3.05 Å (Table 3), below the reported van der Waals contact distance (3.2 Å). In addition, the protonated tertiary amine cation is within 4.1 Å of the ferric trication. Despite this crowding, and in TREN-based analogues possible electrostatic repulsion, tris-salicylato complexes Fe[H_3enterobactin] and analogues such as Fe[H_3MECAM] are stable species.

Conclusion

While iron release from ferric enterobactin proceeds via esterase destruction of the ligand, analogues provide enough iron to support growth of the bacterium despite being impervious to an esterase.[15] This requires an alternative, if minor, pathway for iron release. The new ligands TRENSAM and TREN(3M)SAM form tris-salicylate complexes with Fe^{3+} and Al^{3+}. These complexes support a previously suggested mechanism in which an enterobactin analogue becomes sequentially protonated, adopting a tris-salicylate mode of binding, with subsequent iron release facilitated by a biological reductant. In addition, the spectroscopic and thermodynamic properties of the ferric complexes of TRENSAM and TREN(3M)SAM closely parallel those of Fe[H_3enterobactin], confirming that the latter is a tris-salicylate complex. Their transport properties as substrates for the FepA receptor protein are being investigated separately.

Experimental Section

General. Unless otherwise noted, starting materials were obtained from commercial suppliers and used without further purification. Tris(2-aminoethyl)amine was distilled under vacuum over CaH_2. Flash silica gel chromatography was performed with Merck silica gel, 40−70 mesh. Microanalyses were performed by the Microanalytical Services Laboratory, College of Chemistry, University of California, Berkeley. Mass spectra were recorded at the Mass Spectrometry Laboratory, College of Chemistry, University of California, Berkeley. ^{1}H NMR spectra were recorded on either AMX 300 or AMX 400 Bruker superconducting Fourier transform spectrometers. All ^{13}C NMR were recorded on an AMX 400 Bruker superconducting Fourier transform spectrometer. Infrared spectra were measured with a Nicolet Magna IR 550 Fourier transform spectrometer. Diffuse reflectance UV−vis spectra were recorded on a Lambda 9 Perkin-Elmer double beam spectrophotometer with a dry barium sulfate integrating sphere.

2-Hydroxybenzoylmethylamide (MSAM, 1). To a cooled solution (ice bath) of 40% methylamine (210 mmol) in water was added methyl salicylate (40 mmol) dissolved in 10 mL of MeOH. The formation of a white precipitate was observed. The solution was evaporated to dryness to get a inhomogeneous oil. The oil was purified on a silica plug eluted with 0−1% MeOH/CH_2Cl_2. The solvent was removed and the remaining white solid was recrystallized from hot water, giving colorless crystals. Yield: 30%. IR (film from CH_2Cl_2) ν 1497, 1591, 3407 cm^{-1}. ^{1}H NMR (300 MHz, $CDCl_3$, 25 °C) δ 3.03 (d, $^3J = 9.9$ Hz, 3H, C*H*$_3$), 6.30 (s br, 1H, N*H*), 6.84 (t, $^3J = 7.3$ Hz, 1H, Ar*H*), 7.00 (d, $^3J = 7.5$ Hz, 1H, Ar*H*), 7.36 (m, 2H, Ar*H*), 9.13 (s, 1H, O*H*). ^{13}C NMR (400 MHz, $CDCl_3$, 25 °C) δ 26.4 (CH_3), 114.3 (Ar), 118.5 (Ar), 118.7 (Ar), 125.4 (Ar), 134.2 (Ar), 161.3 (Ar*C*O), 170.7 (*C*═O). Anal. Calcd (Found) for $C_8H_9NO_2$: C, 63.57 (63.46); H, 6.00 (6.04); N, 9.27 (9.19).

2-Methoxybenzoic Acid (2). Salicylic acid (16 mmol), K_2CO_3 (40 mmol), and methyl iodide (35 mmol) **[Caution: methyl iodide is highly toxic]** were stirred in 30 mL of DMF and heated to 90 °C overnight. The reaction mixture was filtered and the filtrate evaporated in vacuo to give a white solid. The solid was purified by flash silica chromatography eluted with CH_2Cl_2. After removal of solvent, the methyl ester intermediate was isolated as an amber oil, which was hydrolyzed in 3 h with 15 mL of MeOH and 10 mL of 6 M NaOH solution. The solution was evaporated to dryness and the resulting residue was redissolved in water. Acidification with 6 M HCl gave a white solid that was isolated by vacuum filtration. Yield: 66%. IR (film from CH_2Cl_2) ν 1259, 1667, 2950 cm^{-1}. ^{1}H NMR (300 MHz, $CDCl_3$, 25 °C) δ 3.98 (s, 3H, C*H*$_3$), 7.00 (m, 2H, Ar*H*), 7.49 (t, $^3J =$ 8.5 Hz, 1H, Ar*H*), 8.02 (d, $^3J = 7.8$ Hz, 1H, Ar*H*). ^{13}C NMR (400 MHz, $CDCl_3$, 25 °C) δ 56.6 (*C*H$_3$), 111.8 (Ar), 117.5 (Ar), 121.8 (Ar), 133.4 (Ar), 135.1 (Ar), 158.3 (Ar*C*O), 166.3 (*C*═O). Anal. Calcd (Found) for $C_8H_8O_3$: C, 63.15 (63.02); H, 5.30 (5.34).

Me-TRENSAM (3). **2** (6.7 mmol) was dissolved in 10 mL of thionyl chloride and 0.15 mL of DMF. The reaction mixture was stirred under a nitrogen atmosphere overnight. The solution was evaporated to dryness and the residue coevaporated with 2 × 30 mL of $CHCl_3$. The oily residue was dissolved in 20 mL of dry THF and reacted dropwise (10 min) with a solution of TREN (2.0 mmol) and 1 mL of triethylamine dissolved in 30 mL of dry THF. The resulting slurry was stirred for 15 min and filtered, and the filtrate was evaporated to dryness. The residue was purified by column chromatography with silica gel, eluted with 0−4% MeOH in CH_2Cl_2. Evaporation of the eluant gave an amber oil. Yield: 48%. IR (film from $CHCl_3$) ν 1527, 1657, 2944 cm^{-1}. ^{1}H NMR (300 MHz, $CDCl_3$, 25 °C) δ 2.88 (t, $^3J =$ 6.4, 6H, C*H*$_2$), 3.63 (q, $^3J = 6.0$, 6H, C*H*$_2$), 3.74 (s, 9H, C*H*$_3$), 6.76 (d, $^3J = 8.4$, 3H, Ar*H*), 7.02 (t, $^3J = 7.6$, 3H, Ar*H*), 7.36 (t, $^3J = 6.9$, 3H, Ar*H*), 8.08 (br s, 3H, N*H*), 8.15 (d, $^3J = 6.4$, 3H, Ar*H*). ^{13}C NMR (400 MHz, $CDCl_3$, 25 °C) δ 35.7 (*C*H$_2$), 54.8 (*C*H$_2$), 56.0 (*C*H$_3$), 111.3 (Ar), 120.6 (Ar), 120.8 (Ar), 131.7 (Ar), 133.1 (Ar), 157.6 (Ar*C*O), 166.4 (*C*═O). Anal. Calcd (Found) for $C_{30}H_{36}N_4O_6 \cdot 0.5H_2O$: C, 64.62 (64.93); H, 6.69 (6.63); N, 10.05 (9.87).

Tris[(2-hydroxybenzoyl)-2-aminoethyl]amine (TRENSAM, 4). Methyl salicylate (78 mmol) was mixed with distilled TREN (17 mmol). The mixture was sealed and heated to 100 °C overnight. The thick resulting oil was purified on a silica column eluted with 0−4% MeOH in CH_2Cl_2, resulting in a white powder after removal of solvent. Overnight drying in vacuo gave a colorless glass. Yield: 47%. IR (KBr) ν 1543, 1590, 1636 cm^{-1}. ^{1}H NMR (300 MHz, CD_3OD, 25 °C) δ 2.78 (t, $^3J = 6.2$ Hz, 6H, C*H*$_2$), 3.49 (t, $^3J = 6.2$ Hz, 6H, C*H*$_2$), 6.68 (t, $^3J = 7.2$ Hz, 3H, Ar*H*), 6.80 (d, $^3J = 7.4$ Hz, 3H, Ar*H*), 7.23 (t, $^3J = 5.8$ Hz, 3H, Ar*H*), 7.63 (d, $^3J = 6.4$ Hz, 3H, Ar*H*), 8.44 (t br, 3H, N*H*). ^{13}C NMR (400 MHz, CD_3OD, 25 °C) δ 39.0 (*C*H$_2$), 54.6 (*C*H$_2$), 117.1 (Ar), 118.4 (Ar), 120.2 (Ar), 129.0 (Ar), 134.7 (Ar), 160.9 (Ar*C*O), 170.9 (*C*═O). Anal. Calcd (Found) for $C_{27}H_{30}N_4O_6$: C, 64.02 (63.94); H, 5.97 (5.97); N, 11.06 (11.01).

(39) Hider, R. C.; Bickar, D.; Morrison, I. E. G.; Silver, J. *J. Am. Chem. Soc.* **1984**, *106*, 6983.

(40) The several inconsistent earlier reports that mischaracterized the aqueous solution protonation chemistry of ferric enterobactin are not cited here. They are analyzed in detail in ref 24.

(41) SMART, Area-Detector Software Package; Siemens Industrial Automation, Inc.: Madison, WI, 1994.

(42) SAINT, SAX Area-Detector Integration Program v. 4.024; Siemens Industrial Automation, Inc.: Madison, WI, 1994.

(43) SHELXTL, Crystal Structure Analysis Determination Package; Siemens Industrial Automation, Inc.: Madison, WI, 1994.

(44) Franczyk, T. S. Ph.D. Dissertation, University of California at Berkeley, 1991.

(45) Kappel, M.; Raymond, K. N. *Inorg. Chem.* **1982**, *21*, 3437.

(46) Raymond, K. N.; McCormick, J. M. *J. Coord. Chem.* In press.

Fe[TRENSAM] (5). TRENSAM (0.3 mmol) was dissolved in 7 mL of MeOH and 0.2 mL of pyridine. To this was added $FeCl_3$ (0.3 mmol). The solution instantly turned deep red, with rapid precipitation of the product as red crystals. After the solution was stirred for 30 min, the solid was collected by filtration and dried overnight. Yield: 97%. IR (KBr) ν 1537, 1574, 1605 cm^{-1}. (+)-FABMS *m*/*z* 560 [M^+ + H].

Al[TRENSAM] (6). TRENSAM (0.8 mmol) was dissolved in 13 mL of MeOH and 0.2 mL of pyridine. To this was added $AlCl_3$ (0.8 mmol). Within minutes the product precipitated as colorless crystals. After the solution was stirred for 30 min the solid was collected by filtration and dried overnight. Yield: 88%. IR (KBr) ν 1537, 1615 cm^{-1}. ^{1}H NMR (300 MHz, CD_3OD, 25 °C) δ 3.47 (s br, 6H, NCH_2), 3.79 (s br, 3H, CH_2NHCO), 4.15 (s br, 3H, CH_2NHCO), 6.62 (ddd, $^3J_{3,4\text{ or }5,6}$ = 8.1 Hz, $^3J_{4,5}$ = 7.0 Hz, $^4J_{4,6\text{ or }3,5}$ = 1.1 Hz, 3H, Ar$H_{4\text{ or }5}$), 6.82 (dd, $^3J_{5,6\text{ or }3,4}$ = 8.6 Hz, $^4J_{4,6\text{ or }3,5}$ = 1.1 Hz, 3H, Ar$H_{6\text{ or }3}$), 7.32 (ddd, $^3J_{5,6\text{ or }3,4}$ = 8.6 Hz, $^3J_{4,5}$ = 7.0 Hz, $^4J_{3,5\text{ or }4,6}$ = 1.6 Hz, 3H, Ar$H_{5\text{ or }4}$), 7.52 (dd, $^3J_{3,4\text{ or }5,6}$ = 8.1 Hz, $^4J_{3,5\text{ or }4,6}$ = 1.6 Hz, 3H, Ar$H_{3\text{ or }6}$). ^{13}C NMR (400 MHz, CD_3OD, 25 °C) δ 36.8 (*C*H_2), 61.1 (*C*H_2), 114.4 (Ar), 116.8 (Ar), 124.3 (Ar), 128.2 (Ar), 137.0 (Ar), 167.5 (Ar*C*O), 174.1 (*C*═O). (+)-FABMS *m*/*z* 531 [M^+ + H].

2-Benzoxy-3-methoxybenzoic Acid (7). 3-Methoxysalicylic acid (54 mmol), K_2CO_3 (153 mmol), and benzyl chloride (139 mmol) were suspended in 140 mL of DMF. The solution was heated to 95 °C overnight. The solution was filtered, and the filtrate was evaporated to dryness to get a dark oil. The oil was purified through a silica plug eluted with CH_2Cl_2, to liberate the benzyl ester intermediate as an amber oil after removal of solvent. The benzyl ester was hydrolyzed by stirring the oil in 45 mL of methanol diluted with 25 mL of 6 M NaOH. After 3.5 h the reaction was complete. The solution was evaporated to near dryness, diluted with 20 mL of water, and acified with 6 M HCl, precipitating an amber, crystalline solid. Yield: 96%. IR (film from CH_2Cl_2) ν 1486, 1703, 1734 cm^{-1}. ^{1}H NMR (300 MHz, $CDCl_3$, 25 °C) δ 4.04 (s, 3H, CH_3), 5.26 (s, 2H, CH_2), 7.30 (br m, 2H, Ar*H*), 7.42 (br m, 5H, Ar*H*), 7.70 (br m, 1H, Ar*H*). ^{13}C NMR (400 MHz, $CDCl_3$, 25 °C) δ 56.3 (*C*H_3), 65.2 (*C*H_2), 117.4 (Ar), 123.9 (Ar), 125.0 (Ar), 127.0 (Ar), 127.6 (Ar), 128.5 (Ar), 128.9 (Ar), 129.1 (Ar), 129.2 (Ar), 135.1 (Ar), 146.9 (Ar*C*O), 152.3 (Ar*C*O), 165.9 (*C*═O). Anal. Calcd (Found) for $C_{15}H_{14}O_4$: C, 69.76 (70.05); H, 5.46 (5.72).

Tris[(2-benzoxy-3-methoxybenzoyl)-2-aminoethyl]amine (8). 7 (9.4 mmol) was dissolved in 20 mL of thionyl chloride and 0.15 mL of DMF. The reaction mixture was stirred under a nitrogen atmosphere overnight. The solution was evaporated to dryness and the residue coevaporated with 2 × 30 mL of $CHCl_3$. The oily residue was dissolved in 30 mL of dry THF and reacted dropwise (10 min) with a solution of TREN (3.0 mmol) and 1 mL of triethylamine dissolved in 20 mL of dry THF. The resulting slurry was stirred for 10 min and filtered, and the filtrate was evaporated to dryness. The residue was purified by column chromatography with silica gel, eluted with 0−4% MeOH in CH_2Cl_2. Evaporation of the eluant gave a brown oil. Yield: 53%. IR (film from CH_2Cl_2) ν 1538, 1657, 2934 cm^{-1}. ^{1}H NMR (300 MHz, $CDCl_3$, 25 °C) δ 2.28 (t, ^3J = 6.9 Hz, 6H, CH_2), 3.12 (q, ^3J = 6.2 Hz, 6H, CH_2), 3.88 (s, 9H, CH_3), 5.01 (s, 6H, CH_2), 7.03 (d, ^3J = 6.5 Hz, 3H, Ar*H*), 7.12 (t, ^3J = 8.0 Hz, 3H, Ar*H*), 7.30 (m, 15H, Ar*H*), 7.62 (d, ^3J = 7.8 Hz, 3H, Ar*H*), 7.77 (br t, 3H, N*H*). ^{13}C NMR (400 MHz, $CDCl_3$, 25 °C) δ 37.2 (*C*H_2), 52.4 (*C*H_2), 56.0 (*C*H_3), 76.1 (*C*H_2), 115.1 (Ar), 122.5 (Ar), 124.3 (Ar), 127.5 (Ar), 128.5 (Ar), 128.6 (Ar), 128.7 (Ar), 128.8 (Ar), 136.6 (Ar), 136.7 (Ar), 146.3 (Ar*C*O), 152.5 (Ar*C*O), 165.3 (*C*═O).

Tris[(2-hydroxy-3-methoxybenzoyl)-2-aminoethyl]amine (TREN-(3M)SAM, 9). 8 (1.7 mmol) was dissolved in 35 mL of MeOH and 0.5 mL of glacial acetic acid. To this solution was added 10% Pd/C catalyst (10 wt % of **10**). The solution was stirred under a hydrogen atmosphere for 24 h. The solution was filtered, and the filtrate was evaporated to dryness to give a white foam. The foam was purified by column chromatography with silica gel, eluted with 0−5% MeOH in CH_2Cl_2. Evaporation of the eluting solvent gave the product as a white foam. Yield: 75%. IR (film from CH_2Cl_2) ν 1458, 1540, 1587, 1635, 2939 cm^{-1}.^{1}H NMR (300 MHz, $CDCl_3$, 25 °C) δ 2.98 (br s, 6H, CH_2), 3.64 (br s, 6H, CH_2), 3.82 (s, 9H, CH_3), 6.53 (t, ^3J = 8.0 Hz, 3H, Ar*H*), 6.83 (d, ^3J = 12.1 Hz, 3H, Ar*H*), 7.24 (d, ^3J = 5.5 Hz, 3H, Ar*H*), 7.90 (s br, 3H, N*H*). ^{13}C NMR (400 MHz, DMSO-d_6, 25 °C) δ 37.8 (*C*H_2), 53.2 (*C*H_2), 56.2 (O*C*H_3), 115.5 (Ar), 115.7 (Ar), 118.2 (Ar), 119.0 (Ar), 148.9 (Ar*C*O), 151.0 (Ar*C*O), 169.8 (*C*═O). Anal. Calcd (Found) for $C_{30}H_{36}N_4O_9$·1.75MeOH: C, 58.42 (58.72); H, 6.64 (6.15); N, 8.58 (8.18).

Fe[TREN(3M)SAM] (10). 9 (0.16 mmol) was dissolved in 20 mL of MeOH. To this solution was added anhydrous $FeCl_3$ (0.14 mmol) and 0.6 mL of pyridine. The solution turned a deep purple-red color. The reaction mixture was stirred for 30 min. The solution was evaporated to dryness and the remaining purple solid collected. IR (KBr) ν 1435, 1546, 1573, 1592 cm^{-1}.

Al[TREN(3M)SAM] (11). 9 (0.32 mmol) was dissolved in 20 mL of MeOH. To this was added $AlCl_3$ (0.30 mmol) and 1 mL of pyridine. The reaction mixture was stirred for 30 min. The solution was evaporated to dryness and the remaining white solid collected. IR (KBr) ν 1451, 1551, 1584, 1610 cm^{-1}. ^{1}H NMR (300 MHz, DMSO-d_6, 25 °C) δ 2.84 (br s, 6H, CH_2), 3.34 (br s, 6H, CH_2), 3.76 (br s, 9H, CH_3), 6.53 (br m, 3H, Ar*H*), 7.26 (br d, 3H, Ar*H*), 7.40 (br m, 3H, Ar*H*). ^{13}C NMR (400 MHz, DMSO-d_6, 25 °C) δ 34.6 (*C*H_2), 55.6 (*C*H_2), 56.3 (O*C*H_3), 114.0 (Ar), 115.5 (Ar), 118.6 (Ar), 119.9 (Ar), 151.9 (Ar*C*O), 157.1 (Ar*C*O), 171.3 (*C*═O).

Structure Solution and Refinement. All X-ray structure data sets were collected on a Siemens SMART area detector diffractometer.[41] Crystals were mounted on quartz capillaries in Paratone oil and were cooled in a nitrogen stream on the diffractometer. Peak integrations were performed with the Siemens SAINT software package.[42] Space group determinations were done by the software XPREP. The structures were solved by direct methods and refined with the SHELXTL software package (PC version).[43] All hydrogen atoms were fixed at calculated positions and their thermal parameters refined isotropically; all non-hydrogen atoms were refined anisotropically.

Fe[TRENSAM] (5). Fe[TRENSAM] crystallized as red plates from a methanol solution of the complex diffused with pentane. The hydrogen on the TREN scaffold was found during the refinement. One molecule of methanol is in the asymmetric unit of the crystal.

Al[TRENSAM] (6). Al[TRENSAM] crystallized as colorless, thin plates from a concentrated methanol solution of the complex diffused with pentane. It is isostructural with the Fe^{3+} complex. The hydrogen on the TREN scaffold was found during the refinement. One molecule of methanol is in the asymmetric unit of the crystal.

Fe[TREN(3M)SAM] (10). Fe[TREN(3M)SAM] crystallized as purple blocks from a methanol solution of the complex diffused with diethyl ether. One molecule of pyridine, 2.5 (two full occupancy and one-half occupancy) water molecules, and 5 methanol molecules were found in the asymmetric unit. The disorder of some of the solvent molecules limited the quality of the refinement.

Al[TREN(3M)SAM] (11). Al[TREN(3M)SAM] crystallized as light pink blocks from a concentrated methanol solution of the complex diffused with pentane. The hydrogen on the TREN scaffold was found during the refinement. Two molecules of methanol and one pyridinium chloride are in the asymmetric unit.

Variable-Temperature ^{1}H NMR Measurements. Variable-temperature ^{1}H NMR experiments were carried out in the range 265−335 K on a Bruker AMX 300 spectrometer operating at 300 MHz. The temperature was controlled by the B-VT2000 equipment of the spectrometer that ensures a precision of ±1 K. The probe temperature was allowed to equilibrate for 10 min prior to final magnetic homogeneity optimization on the lock signal. Variation at a given temperature was less than ±0.1 K. The spectra were recorded in CD_3OD (Aldrich, % D > 99.8). The sample concentration was approximately 15 mM. All chemical shifts were referenced to the solvent peak.

Solutions Thermodynamics. General Methods. All titrant solutions were prepared with distilled water that was further purified by passing through a Millipore Milli-Q reverse osmosis cartridge system (resistivity 18 MΩ cm) and then degassed by boiling for 1 h while being purged by argon. Titrant solutions were stored under an atmosphere of purified argon with Ridox Oxygen Scavenger (Fisher) and Ascarite II (A. H. Thomas) scrubbers to prevent absorption of oxygen and carbon dioxide. Carbonate-free 0.1 M KOH was prepared from Baker Dilut-It concentrate and standardized by titrating against

potassium hydrogen phthalate with phenolphthalein as an indicator. Solutions of 0.1 M HCl were similarly prepared and standardized by titrating against the KOH solution to phenolphthalein endpoint. The combined pH glass electrode (Orion semimicro) filled with 3 M KCl (Orion filling solution) was calibrated in hydrogen ion concentration units (p[H] = $-\log [H^+]$) by titrating 2.000 mL of standardized HCl diluted in 50 mL of 0.100 M KCl (Mallinckrodt, ACS grade) with 4.200 mL of standardized KOH. The Nernst parameters of the electrode and the pK_w value (13.78 ± 0.05) were refined with a nonlinear least-squares program.[44,45] Solutions were maintained under argon atmosphere at constant ionic strength (I = 0.1 KCl) and temperature (25.0(2) °C) by using a jacketed titration vessel fitted to a Lauda K-2/R water bath. The thermodynamic reversibility was checked by cycling the titrations from low to high p[H] and vice versa. All results presented are the average of at least three independent titrations.

Potentiometric Titrations. All titrations were performed with a Dosimat 665 (Metrohm) piston buret and an Accumet 925 (Fisher) pH meter, both instruments being controlled by an IBM-PC computer.[32] The models used to fit the titration data were refined by the weighted nonlinear least-squares program BETA90.[44] In the final refinement step, the total amount of titrated ligand was also allowed to vary. The standard deviations of the stepwise protonation constants (log K_a's) were derived from the full variance/covariance matrix of the refined global constants (log β's).[46]

Spectrophotometric Titrations. The apparatus and methods for spectrophotometric titrations have been described in detail elsewhere.[28] The path length of the used quartz cell (Hellma, Suprasil) was 10 cm. To 50 mL of 0.100 M KCl, an aliquot of a freshly prepared solution in *N*,*N*-dimethylacetamide (Fisher) of the titrated compound was added. The effect of the added solvent was neglected, the final concentration being less than 0.4%. After the p[H] was raised to about 11.5 with 0.1 M KOH, the ligands were titrated with standardized 0.1 M HCl. For the complexes no base was added. The data (including absorbances at different wavelengths, p[H] values, and respective volumes of solutions) were analyzed by the factor analysis program FINDCOMP prior to the nonlinear least-squares refinement of the stability constants and extinction coefficients by the program REFSPEC.[28]

^{1}H NMR Titration. A 7.5 mM solution of TREN(3M)SAM in basic D_2O (Aldrich, % D > 99.9) was titrated at room temperature and under nitrogen atmosphere by adding small amounts of ca. 5% diluted DCl (Aldrich, 20 wt %, % D > 99.5) solutions in D_2O with a Gilmont micropipet. After each titrant addition, a ca. 0.5 mL aliquot was taken from the titration vessel. Apparent p[H] values were measured with a semimicroelectrode (Orion) filled with 3 M KCl fitted to an Accumet 925 (Fisher) pH meter. The electrode was calibrated in water with proton concentration units as described in the general methods section. The corrected p[D] values were calculated according to the formula p[D] = p[H]$_{mes}$ + 0.4.[36] The NMR spectra were recorded on a 300 MHz Bruker AMX 300 spectrometer and referenced to acetonitrile (δ = 1.95 ppm). Protonation constants were refined by a nonlinear least-squares program with the Simplex algorithm and corrected for the deuterium effect according to the correlation by Delgado et al.: log K^D = 0.32 + 1.044 log K^H.[35]

Acknowledgment. We thank Drs. Fred Hollander and Ryan Powers for assistance with the X-ray structure determinations, Dr. Jide Xu for helpful discussions, and Christopher J. Sunderland for a gift of starting material. This work was supported by NIH Grant No. AI11744.

Supporting Information Available: Tables of crystal data, atomic coordinates, bond lengths and angles, anisotropic displacement parameters, and hydrogen coordinates (5 pages, print/PDF). See any current masthead page for ordering and Web access instructions.

JA973442S